SPOP is essential for DNA–protein cross-link repair in prostate cancer cells: SPOP-dependent removal of topoisomerase 2A from the topoisomerase 2A-DNA cleavage complex

Ryuta Watanabe[a,b,†], Masashi Maekawa[b,c,†,*], Miki Hieda[d], Tomohiko Taguchi[e], Noriyoshi Miura[a], Tadahiko Kikugawa[a], Takashi Saika[a], and Shigeki Higashiyama[b,c,*]

[a]Department of Urology and [b]Department of Biochemistry and Molecular Genetics, Ehime University Graduate School of Medicine, and [c]Division of Cell Growth and Tumor Regulation, Proteo-Science Center, Ehime University, Shitsukawa, Toon, Ehime 791-0295, Japan; [d]Graduate School of Health Sciences, Ehime Prefectural University of Health Sciences, Takoda, Tobe-cho, Iyo-gun, Ehime 791-2101, Japan; [e]Department of Integrative Life Sciences, Graduate School of Life Sciences, Tohoku University, Aoba-Ku, Sendai 980-8577, Japan

ABSTRACT SPOP, speckle-type POZ protein is a substrate adaptor protein of the Cullin-3/RING ubiquitin E3 complex. The *spop* gene is the most commonly point mutated in human primary prostate cancers, but the pathological contribution of the SPOP mutations remains unclear. In this study, we investigated several known factors that are critical in the DNA–protein cross-link repair process. The depletion of SPOP or overexpression of a prostate cancer–associated SPOP mutant, F133V, in androgen receptor-positive prostate cancer cells increased the amount of topoisomerase 2A (TOP2A) in the nuclei together with the increased amount of γH2AX, an indication of DNA breaks. Tyrosyl–DNA phosphodiesterases (TDPs) and an endo/exonuclease MRE11 are enzymes that liberate TOP2A from the TOP2A–DNA cleavage complex, and thus is essential for the completion of the DNA repair process. We found that the amount of TDP1 and TDP2 was decreased in SPOP-depleted cells, and that of TDP2 and MRE11 was decreased in F133V-overexpressing cells. These results suggest that the F133V mutant exerts dominant-negative and gain-of-function effects in down-regulation of TDP2 and MRE11, respectively. We conclude that SPOP is involved in the DNA–protein cross-link repair process through the elimination of TOP2A from the TOP2A cleavage complex, which may contribute to the genome stability.

INTRODUCTION

SPOP (speckle-type POZ protein) is a substrate recognizing receptor of the cullin-3 (CUL3)/RING ubiquitin E3. Heterozygous point mutations in the substrate-binding domain (MATH domain) of SPOP have been frequently found in 10–15% of recurrent human prostate cancer patients (Barbieri *et al.*, 2012). Prostate cancer–associated

SPOP mutants such as Y87C and F133V fail to interact with its substrates (e.g., androgen receptor [AR], ERG, DAXX, DEK, TRIM24), and expression of these SPOP mutants impairs ubiquitination of the substrates leading to the inhibition of their proteasomal degradation (Kwon *et al.*, 2006; An *et al.*, 2014; Theurillat *et al.*, 2014;

epidermal growth factor; EGFR, epidermal growth factor receptor; H2AX, H2A histone family member X; HDR, homology-directed repair; NHEJ, nonhomologous end joining; PSA, prostate-specific antigen; SPOP, speckle-type POZ protein; SSB, single-strand break; TDP, tyrosyl–DNA phosphodiesterases; TOP, topoisomerase; Ub, ubiquitin; UV, ultraviolet.

Gan et al., 2015; Cheng et al., 2018). Recent studies have identified critical functions of SPOP in DNA repair and genome stability in response to exogenous DNA damage stresses in prostate cancer cells (Boysen et al., 2015; Hjorth-Jensen et al., 2018). Knockdown of SPOP or overexpression of the prostate cancer–associated SPOP mutant, F133V, resulted in impaired homology-directed repair (HDR) and promoted nonhomologous end joining (NHEJ) after γ-irradiation-induced double-strand breaks (DSBs; Boysen et al., 2015). SPOP-depleted prostate cancer cells do not form Rad51-positive foci by treatment of cells with replication stress inducers (hydroxyurea and camptothecin) or by ultraviolet (UV) irradiation (Hjorth-Jensen et al., 2018). The reduced levels of mRNAs that code DNA repair-related proteins by SPOP knockdown may account for the defects of DNA repair in response to exogenous DNA damage stresses (Boysen et al., 2015; Hjorth-Jensen et al., 2018).

In addition to the exogenous DNA damage response, DNA repair machinery is involved in the endogenous DNA damage response that inevitably occurs during the DNA replication process in the S phase (Bartek et al., 2004). In this process, the emergence of supercoiled and catenated DNA is one of the problematic DNA replication stresses (Gaillard et al., 2015). To remove the distortions in the newly replicated DNA, both topoisomerase 1 (TOP1) and topoisomerase 2 (TOP2) form covalent DNA–protein cross-link called protein adducts, and frequently introduce transient single-strand breaks (SSBs) and DSBs, respectively (Pommier et al., 2016; Stingele et al., 2017). The DNA–protein cross-link repair is thus necessary for the completion of accurate DNA replication and subsequent chromosome segregation (Pommier et al., 2016). After introduction of DNA breaks, the TOP1 or TOP2 is eliminated from the TOP cleavage complex by the tyrosyl–DNA phosphodiesterase 1 (TDP1) or TDP2, which cleaves phosphotyrosyl bonds between the DNA and the tyrosine residue of TOP1 or TOP2, respectively (Pommier et al., 2014). An endo/exonuclease MRE11 forms a complex with Rad50 and NBS1, and the MRN complex (MRE11/RAD50/NBS1) removes the TOP2–DNA complex by the endonucleolytic cleavage followed by a second cut on the complementary strand (Stingele et al., 2017). The MRN complex is necessary for the phosphorylation of ataxia telangiectasia–mutated (ATM) to proceed with the HDR and NHEJ, which complete the DSB repair (Lee and Paull, 2004, 2005).

To date, roles of SPOP during DNA repair in response to exogenous DNA damage stresses have been characterized (Boysen et al., 2015; Hjorth-Jensen et al., 2018); however, it remains unclear whether SPOP is involved in DNA repair in response to endogenous DNA replication stresses. Here, we analyzed several crucial factors in the DNA–protein cross-link repair process. We found that the protein expression of TDP1 and TDP2 was decreased, and TOP2A was accumulated as the protein adducts with DNA in SPOP-knockdown cells. We also showed that overexpression of a prostate cancer–associated SPOP mutant, F133V, reduced the protein expression of TDP2 and MRE11 together with the accumulation of TOP2A in the nuclei. We suggest that the F133V mutant may serve as a dominant-negative and gain-of-function mutant in downregulation of TDP2 and MRE11, respectively. Our results suggest the novel function of SPOP in regulating TOP2A during DNA replication in AR-positive prostate cancer cells.

RESULTS
Depletion of SPOP increases the level of γH2AX in prostate cancer cell lines in the absence of exogenous DNA damage stresses
To investigate functions of SPOP in DNA repair during DNA replication in normally growing prostate cancer cells, we first examined the level of phosphorylated H2A histone family member X (γH2AX), which indicates the DNA breaks, in various prostate cancer cell lines, including C4-2, LNCaP, PC3, and DU145 cells. These cells harbor wild-type (WT) spop gene. We treated the cells with small interfering RNA (siRNA) oligos designed for SPOP, and knockdown efficiency was confirmed in each cell line by Western blotting (Figure 1A). As shown, the level of γH2AX (the ratio of γH2AX/H2AX) was remarkably elevated in the AR-positive prostate cancer cell lines, C4-2 and LNCaP cells, but not in AR-negative prostate cancer cell lines, PC3 and DU145 cells, upon SPOP knockdown (Figure 1, A and B). These data suggest that the depletion of SPOP causes accumulation of the DNA breaks in AR-positive prostate cancer cells in response to endogenous DNA damage stresses. As shown in Figure 1A and Supplemental Figure S1A, SPOP knockdown reduced the protein expression level of H2AX, checkpoint kinase 2 (ChK2), and ATM in C4-2, LNCaP, and PC3 cells, which would be accounted by a previous study showing that SPOP knockdown reduced the mRNA level of ChK2 in prostate cancer cells (Hjorth-Jensen et al., 2018). We also showed that the mRNA level of H2AX was significantly reduced by SPOP knockdown in C4-2 cells (Supplemental Figure S1B). During exposure to DNA damage stresses such as irradiation with UV or γ-rays, γH2AX formation is mediated through the ATM/ChK2 pathway (Smith et al., 2010). However, neither the increased phosphorylation of ATM (pATM) nor that of ChK2 (pChK2) was detected in each SPOP-depleted cell line (Figure 1, A and B). These data suggest that neither ATM nor ChK2 is activated upon SPOP knockdown. Treatment of SPOP-depleted C4-2 cells with an ATM inhibitor, Ku55933, did not affect the level of γH2AX, suggesting the ATM-independent generation of γH2AX in SPOP-knockdown cells (Supplemental Figure S2, A–C). As the markedly increased levels of γH2AX by SPOP knockdown were observed in AR-positive cell lines, C4-2 and LNCaP cells, we further analyzed SPOP-mediated molecular events using C4-2 cells. The SPOP knockdown significantly increased the formation of γH2AX-positive foci in the nuclei of C4-2 cells (Figure 1, C and D). The expression of siRNA-resistant nontagged WT SPOP reduced the level of γH2AX in SPOP-knockdown cells, excluding the off-target effect of siRNA (Figure 1, E and F). DNA replication is promoted by the stimulation with growth factors such as epidermal growth factor (EGF; Miskimins et al., 1983). As shown, the level of γH2AX in SPOP-depleted cells was slightly increased by incubation with EGF for 24 h (Supplemental Figure S2, D and E). Taken together, these data suggest that SPOP is involved in the replication-coupled DNA damage response in AR-positive prostate cancer cells.

Topoisomerase inhibitors do not increase the level of γH2AX in SPOP-knockdown cells
Topoisomerases (TOPs) are endogenous replication stress inducers (Gaillard et al., 2015). Because SPOP knockdown caused the accumulation of DNA breaks in the absence of exogenous DNA damage stresses (Figure 1), we thus reasoned that SPOP regulates TOPs during DNA replication. To examine the relationship between TOPs and SPOP, we treated control or SPOP-depleted–C4-2 cells with TOP inhibitors. A topoisomerase 1 (TOP1) inhibitor, irinotecan, and a topoisomerase 2 (TOP2) inhibitor, etoposide, trap each enzyme on the cleaved site of DNA by the formation of cytotoxic covalently linked TOP1 or TOP2 adducts on DNA, resulting in the generation of SSBs or DSBs and abrogation of DNA repair (Delgado et al., 2018). We also treated cells with hydroxyurea (a potent ribonucleotide reductase inhibitor) which causes lack of deoxyribonucleotides, resulting in the inhibition of both DNA replication and DNA repair (Koc et al., 2004). As shown, all of these inhibitors increased the levels of both γH2AX
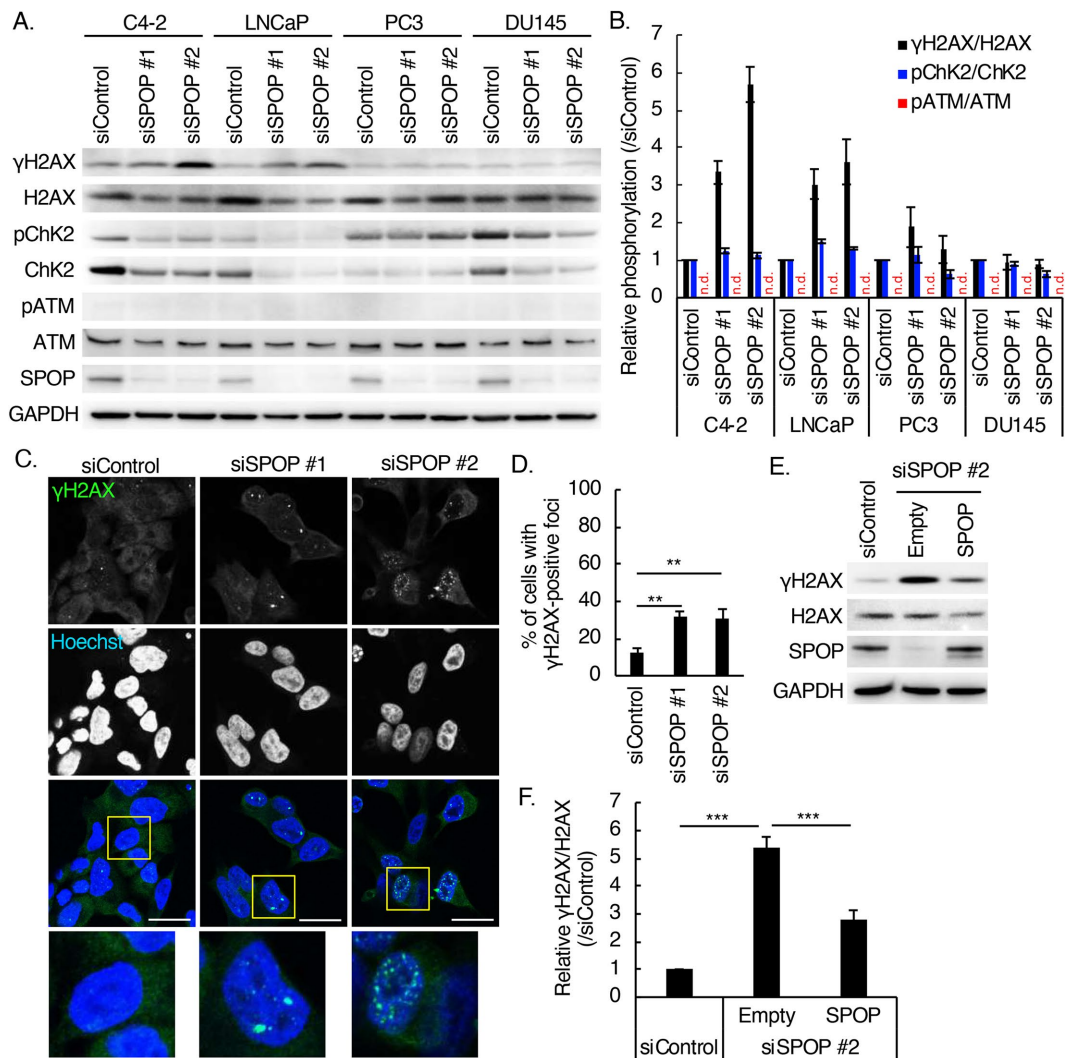
FIGURE 1: SPOP knockdown elevated the level of γH2AX in the absence of DNA damage stresses in AR-positive prostate cancer cells. (A) Western blots of C4-2, LNCaP, PC3, and DU145 cell lysates 72 h posttransfection of siRNAs. (B) Quantitation of A. The ratio of γH2AX/H2AX, pATM/ATM, and pChK2/ChK2 from three independent experiments was analyzed. Data show the mean ± SEM. n.d., not detected. (C) Confocal images of C4-2 cells fixed after 72 h of siRNA transfection, permeabilized, and stained for γH2AX antibody. Magnifications of the yellow squared areas are shown in the bottom panels. Bars = 20 µm. (D) Quantitation of C. Cells with γH2AX-positive foci were counted. In total, 100 cells from three independent experiments were analyzed. Data show the mean ± SEM. **, $p < 0.01$. (E) Rescue experiments of SPOP knockdown. Western blots of C4-2 cell lysate infected with siRNA-resistant–nontagged SPOP WT-carrying lentivirus. Empty, control lentivirus. (F) Quantitation of E. Ratio of γH2AX/H2AX from three independent experiments was analyzed. Data show the mean ± SEM. ***, $p < 0.001$; Empty, control lentivirus.

and pATM in control C4-2 cells in a dose-dependent manner (Figure 2, A–C). In contrast, these inhibitors did not significantly increase the level of γH2AX in SPOP-depleted C4-2 cells (Figure 2, A–C). These data suggest that SPOP knockdown causes the accumulation of TOP1 or TOP2 as protein adducts with DNA, resulting in the inhibition of DNA–protein cross-link repair.

Topoisomerase 2A is accumulated on cleaved DNA in SPOP-knockdown cells

To investigate functions of SPOP in regulating TOP or TOP2, we first assessed the TOP1 and TOP2 activities in vitro upon SPOP knockdown (Figure 3, A and B). As shown, the relaxed-coiled DNA was detected by incubation of supercoiled DNA with 1 µg of control or SPOP-knockdown nuclear lysates (Figure 3A and Supplemental Figure S3A). We also observed the generation of decatenated

kinetoplast DNA (kDNA) by incubation of catenated kDNA with 0.1, 0.5, or 1 µg of control or SPOP-knockdown nuclear lysates (Figure 3B and Supplemental Figure S3B). Treatment of control or SPOP-knockdown nuclear lysates with etoposide generated linear kDNA in addition to nicked open circular and relaxed circular DNAs (Supplemental Figure S3C) as reported previously (Lee *et al.*, 2012a). These data suggest that both free TOP1 and TOP2 in the nuclei are still enzymatically active in SPOP-knockdown cells. We next examined the expression and subcellular localization of TOPs in control and SPOP-knockdown C4-2 cells. TOP1 and TOP2A were dominantly expressed compared with TOP2B in control C4-2 cells, and SPOP depletion slightly reduced the protein expression of TOP2A without affecting that of TOP1 (Figure 3, C and D). Nuclear localization of TOP1 and TOP2A was observed in SPOP-knockdown cells as in the control C4-2 cells (Figure 3E and Supplemental Figure
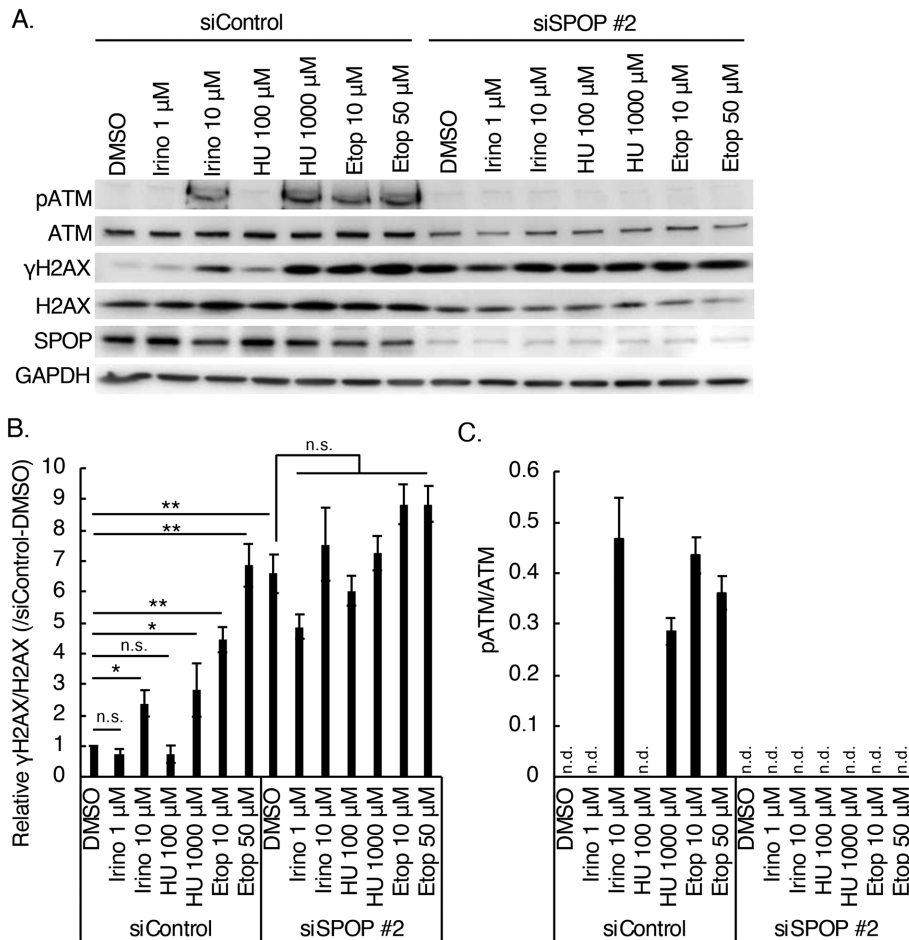
FIGURE 2: Increased level of γH2AX by depletion of SPOP was not enhanced by topoisomerase inhibitors and hydroxyurea. (A) Western blots of cell lysates prepared from control or SPOP-knockdown C4-2 cells incubated with inhibitors of DNA repair. Cells were treated with irinotecan (Irino), hydroxyurea (HU), or etoposide (Etop) at the indicated concentrations in 10% FBS–containing medium for 24 h. (B) Quantitation of A. The ratio of γH2AX/H2AX was analyzed from three independent experiments. Data show the mean ± SEM. *, $p < 0.05$; **, $p < 0.01$; n.s., not significant. (C) Quantitation of A. Ratio of pATM/ATM from three independent experiments was analyzed. Data show the mean ± SEM. n.d., not detected.

S4A). Of note, the fluorescence intensity of TOP2A in the nuclei was significantly increased by SPOP knockdown (Figure 3, E and F). In contrast, the fluorescence intensity of TOP1 in the nuclei was not changed in SPOP-knockdown C4-2 cells (Supplemental Figure S4, A and B). We then biochemically isolated the DNA–protein complex by cesium chloride-density gradient centrifugation and detected by dot blotting with anti-TOP2A antibody according to the previous report (Hoa *et al.*, 2016). In this assay, the TOP2A–DNA cleavage complex was fractionated to the lower cesium chloride gradient fractions. We detected the increased TOP2A–DNA cleavage complex in etoposide-treated C4-2 cells in the lower fractions compared with the control as shown previously (Figure 3, G and H, fraction #'s 4–6; Hoa *et al.*, 2016). We also confirmed that treatment of C4-2 cells with mirin, a MRE11 nuclease inhibitor (Dupre *et al.*, 2008; Lee *et al.*, 2012b), caused the accumulation of TOP2A–DNA cleavage complex in the lower fractions (Figure 3, G and H, fraction #'s 4 and 5). These data suggested that the assay can detect the inhibition of removal of TOP2A from the TOP2A–DNA cleavage complex. In SPOP-depleted C4-2 cells, we detected the accumulation of the TOP2A–DNA cleavage complex in the lower fraction compared

with that from control C4-2 cells (Figure 3, G and H, fraction #4), which was similar to the fractionation pattern of mirin-treated cells, suggesting that SPOP would be required for removal of TOP2A from the TOP2A–DNA cleavage complex. Covalently bound TOP2A on chromosomal DNA are eliminated by tyrosyl–DNA phosphodiesterases (TDP1 and TDP2) and an endo/exonuclease (MRE11; Stingele *et al.*, 2017). The protein expression level of both TDP1 and TDP2 in SPOP-depleted C4-2 cells was reduced approximately 50% compared with that of the control cells without affecting their mRNA expression (Figure 3, I–K). Although SPOP knockdown reduced the mRNA expression of MRE11, its protein expression was not affected by SPOP knockdown in C4-2 cells (Figure 3, I–K). Because TDP1 can cleave TOP2A from genomic DNA as well as TDP2 (Murai *et al.*, 2012), the reduced protein levels of TDP1 and TDP2 in SPOP-depleted cells may result in insufficient removal of TOP2A from its DNA adduct, or accumulation of TOP2A on genomic DNA.

Transient overexpression of a prostate cancer–associated SPOP mutant, F133V, causes the accumulation of γH2AX and TOP2A in nuclei

We next examined the pathological significance of prostate cancer–associated SPOP mutants in the DNA–protein cross-link repair process. To this end, we transiently expressed nontagged WT SPOP and prostate cancer–associated SPOP mutants, Y87C or F133V, in C4-2 cells (Figure 4A). We observed the increased level of γH2AX by overexpression of the F133V mutant but not by overexpression of WT or Y87C mutant (Figure 4, A and B). Both protein and mRNA expression of H2AX were reduced by over-

expression of the F133V mutant (Figure 4A and Supplemental Figure S5, A and B). Overexpression of WT or Y87C mutant decreased mRNA level of H2AX without affecting its protein expression (Figure 4A and Supplemental Figure S5, A and B). Consistent with the Western blotting (Figure 4A), overexpression of the F133V mutant alone significantly increased the formation of γH2AX-positive foci in the nuclei of C4-2 cells (Figure 4, C and D). Protein expression of ATM and ChK2 was not affected by any overexpression of WT, Y87C, or F133V mutants (Figure 4A and Supplemental Figure S5A), and neither pATM nor pChK2 was elevated in any overexpressors tested here (Figure 4, A and B). These data suggest that the increased level of γH2AX in F133V mutant–overexpressing C4-2 cells is independent of the ATM/ChK2 pathway as was seen in SPOP-depleted C4-2 cells.

We further investigated the protein expression and cellular localization of TOP1 and TOP2A in SPOP-overexpressing cells. Overexpression of WT or Y87C mutant did not affect the protein expression of TOP1 and TOP2A in C4-2 cells, whereas overexpression of the F133V mutant increased the protein expression of TOP2A but not TOP1 (Figure 4A and Supplemental Figure S5A). The fluorescence
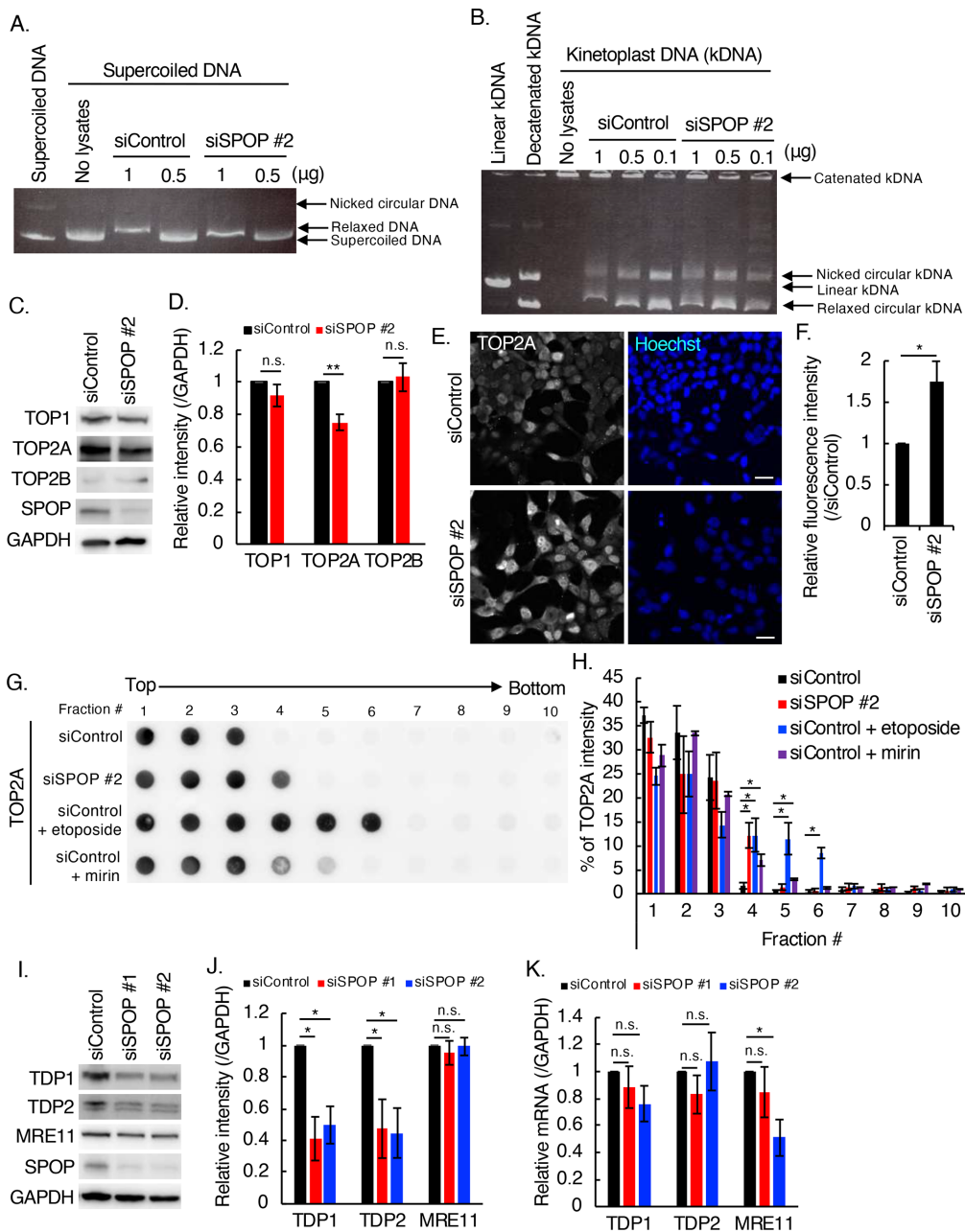
FIGURE 3: SPOP knockdown increased the topoisomerase 2A–DNA cleavage complex during DNA replication in C4-2 cells. (A) Topoisomerase 1 (TOP1) activity assay. Lysates extracted from the nuclear pellets were incubated with supercoiled DNA for 30 min at 37°C in the absence of ATP, and subjected to electrophoresis. Relaxed DNA was shifted upward compared with supercoiled DNA. (B) Topoisomerase 2 (TOP2) activity assay. Lysates extracted from the nuclear pellets were incubated with catenated kinetoplast DNA (kDNA) for 30 min at 37°C in the presence of ATP, and subjected to electrophoresis. Decatenated kDNA were detected as two bands (nicked circular kDNA and relaxed circular kDNA). (C) Western blots of C4-2 cell lysates 72 h posttransfection of siRNAs. (D) Quantitation of C. The ratio of TOP1/GAPDH, TOP2A/GAPDH, and TOP2B/GAPDH was analyzed from three independent experiments. Data are normalized to siControl. Data show the mean ± SEM. **, $p < 0.01$; n.s., not significant. (E) Confocal images of C4-2 cells fixed after 72 h of siRNA transfection, permeabilized, and stained for TOP2A antibody. Bars = 20 µm. (F) Quantitation of E. Fluorescence intensity of TOP2A in the nuclei was measured and normalized to that of control cells. In total, 100 cells from three independent experiments were analyzed. Data show the mean ± SEM. *, $p < 0.05$. (G) Western dot blot analysis of purified genomic DNA fractionated by cesium chloride–density gradient centrifugation. C4-2 cells were treated with etoposide (10 µM) or mirin (100 µM) in 10% FBS–containing medium for 2 or 4 h, respectively, before cell lysis. (H) Quantitation of G. The blot intensity of each fraction (#'s 1–10) was shown as the percentage of total blot intensity. Data show the mean ± SEM from three independent experiments. *, $p < 0.05$. (I) Western blots of C4-2 cell lysates 72 h posttransfection of siRNAs. (J) Quantitation of I. The ratio of TDP1/GAPDH, TDP2/GAPDH, and MRE11/GAPDH was analyzed from three independent experiments. Data are normalized to siControl. Data show the mean ± SEM. *, $p < 0.05$; n.s., not significant. (K) The mRNA level of TDP1, TDP2, and MRE11 from four independent experiments was analyzed by RT-PCR. Data are normalized to siControl. Data show the mean ± SEM. *, $p < 0.05$; n.s., not significant.
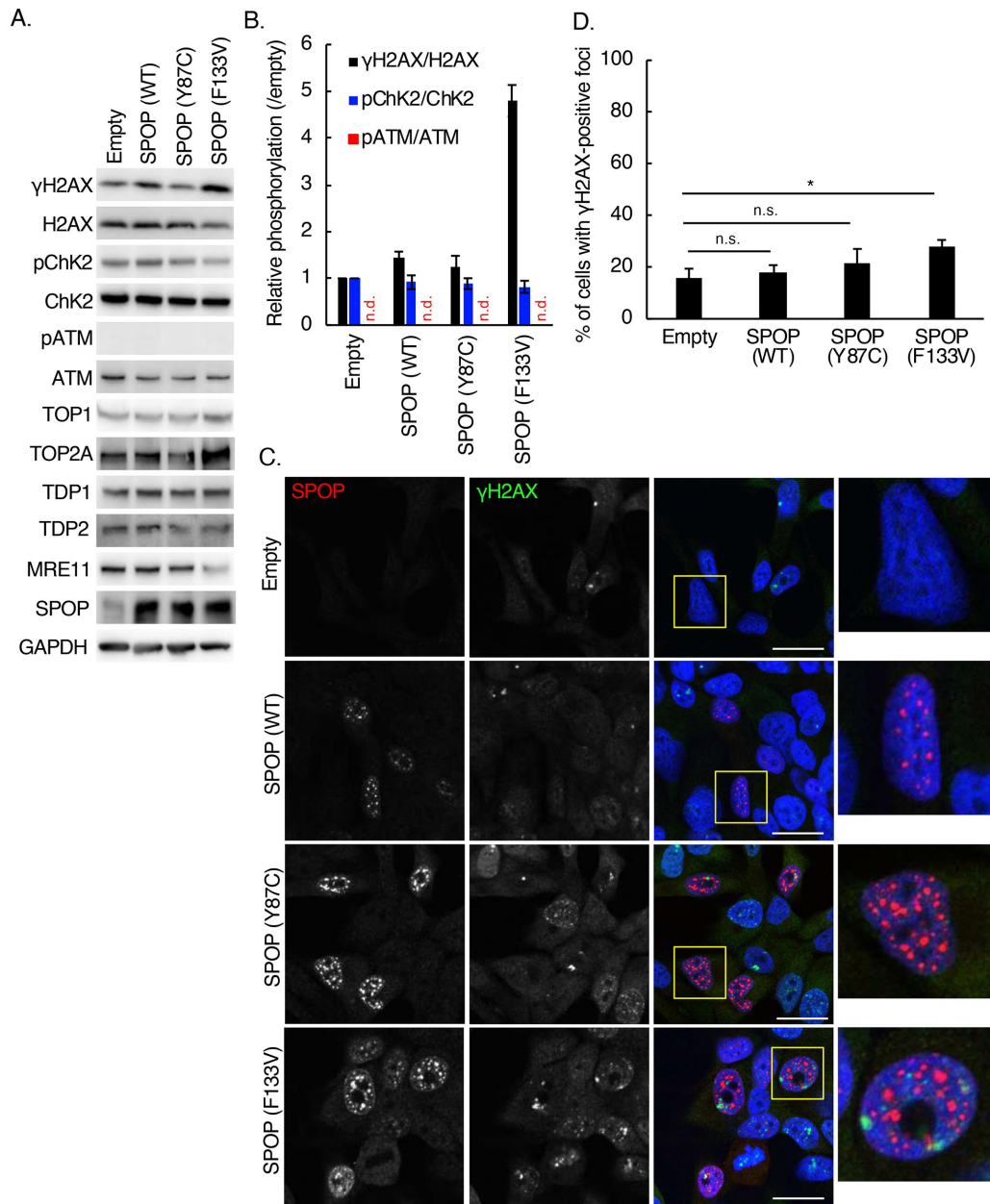
FIGURE 4: Enforced overexpression of a prostate cancer–associated SPOP mutant, F133V, increased the level of γH2AX in C4-2 cells. (A) Western blots of C4-2 cell lysates 96 h after infection of nontagged SPOP WT, Y87C, or F133V mutant-carrying lentivirus. Empty, control lentivirus. (B) Quantitation of A. The ratio of γH2AX/H2AX, pATM/ATM, and pChK2/ChK2 from three independent experiments was analyzed. Data show the mean ± SEM. n.d., not detected. Empty, control lentivirus. (C) Confocal images of C4-2 cells fixed after 96 h postlentiviral infection, permeabilized, and stained for γH2AX and SPOP antibody. Magnifications of the yellow squared areas are shown in the right panels. Bars = 20 μm. Empty, control lentivirus. Note that exogenously expressing SPOP was visualized using an anti-SPOP polyclonal antibody, which can recognize not endogenous but overexpressed SPOP in immunostaining. (D) Quantitation of E. Cells with γH2AX-positive foci were counted. In total, 100 cells from three independent experiments were analyzed. The γH2AX-positive foci were analyzed in cells overexpressing SPOP (WT and mutants). Data show the mean ± SEM. *, $p < 0.05$; n.s., not significant; Empty, control lentivirus.

intensity of TOP1 and TOP2A in the nuclei was slightly increased by the overexpression of WT SPOP (Figure 5, A–D). In contrast, we observed the remarkable increase of the fluorescence intensity of TOP2A but not TOP1 in the nuclei by overexpression of the mutants (Y87C or F133V) as was seen in SPOP-knockdown cells (Figure 5, A–D). Overexpression of the F133V mutant increased the fluorescence intensity of TOP2A in the nuclei much more than that of the Y87C mutant did (Figure 5, C and D). Overexpression of the Y87C or

F133V mutant reduced the protein expression of TDP2 but not TDP1 (Figure 4A and Supplemental Figure S5A). Of note, the protein expression of MRE11 was decreased by overexpression of the F133V mutant but not by that of WT or Y87C mutant (Figure 4A and Supplemental Figure S5A). The reduced protein expression of TDP2 and MRE11 may account for the markedly increased protein expression and nuclear immunofluorescence intensity of TOP2A in F133V mutant–overexpressing cells. Taken together with SPOP-knockdown
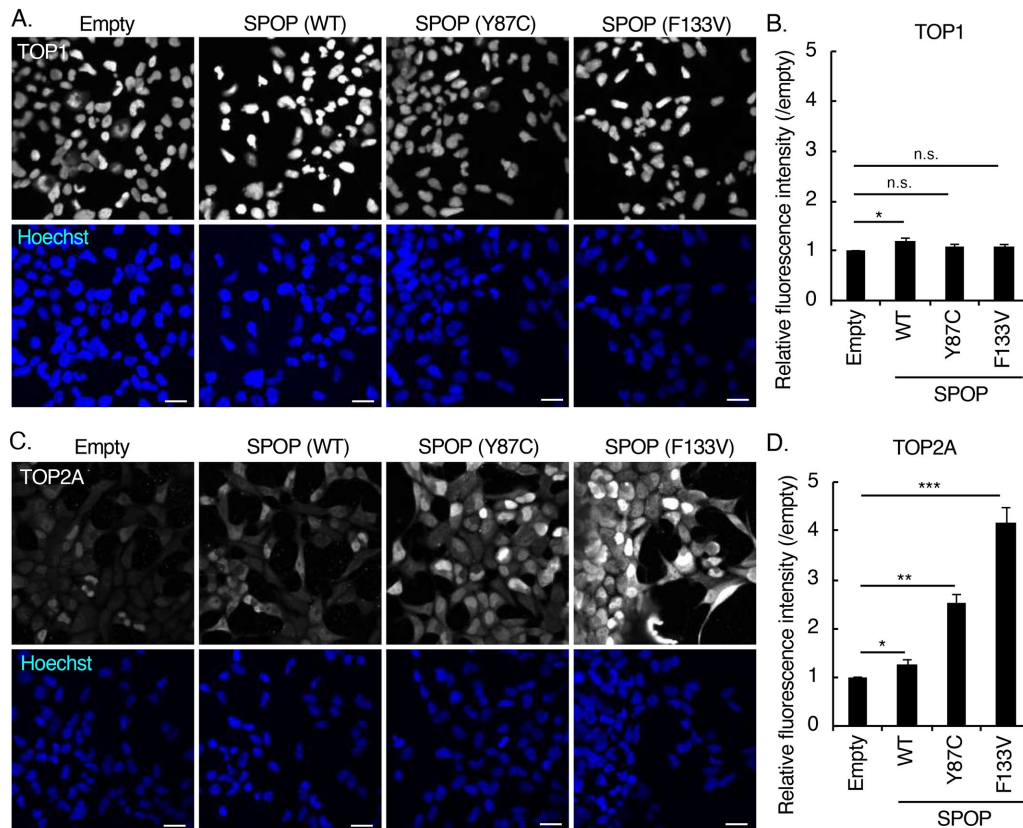
FIGURE 5: Enforced overexpression of a prostate cancer–associated SPOP mutant, F133V, drastically increased the immunofluorescence staining for TOP2A. (A) Confocal images of C4-2 cells fixed after 96 h postlentiviral infection, permeabilized, and stained for TOP1 antibody. Bars = 20 μm. Empty, control lentivirus. (B) Quantitation of A. Fluorescence intensity of TOP1 in the nuclei was measured and normalized to that of control cells. In total, 50 cells were analyzed. Data show the mean ± SEM. *, $p < 0.05$; n.s., not significant; Empty, control lentivirus. (C) Confocal images of C4-2 cells fixed after 96 h postlentiviral infection, permeabilized, and stained for TOP2A antibody. Bars = 20 μm. Empty, control lentivirus. (D) Quantitation of C. Fluorescence intensity of TOP2A in the nuclei was measured and normalized to that of control cells. In total, 50 cells were analyzed. Data show the mean ± SEM. *, $p < 0.05$; **, $p < 0.01$; ***, $p < 0.001$; Empty, control lentivirus.

analysis, these data suggest that the F133V mutant would serve as a dominant-negative mutant in the down-regulation of TDP2 and a gain-of-function mutant in the down-regulation of MRE11. Collectively, it is suggested that overexpression of the F133V mutant causes insufficient removal of TOP2A from its protein adduct resulting in the accumulation of DSBs.

The generation of γH2AX in SPOP-knockdown cells is AR/TOP2A dependent

The markedly elevated level of γH2AX by SPOP knockdown was not observed in AR-negative prostate cancer cell lines, PC3 cells, and DU145 cells (Figure 1, A and B). It is also reported that androgen stimulation induced TOP2-mediated DSBs and the formation of γH2AX-positive foci, leading to gene arrangements in prostate cancers (Haffner *et al.*, 2010; Schaefer-Klein *et al.*, 2015). AR directly interacts with TOP2B upon androgen stimulation, and corecruitment of AR/TOP2B induces TOP2-dependent DSB formation resulting in the accumulation of γH2AX (Haffner *et al.*, 2010). To examine the relationship between AR and increased γH2AX in SPOP-knockdown cells, we blocked AR signaling in SPOP-knockdown C4-2 cells by treatment with an AR inhibitor, enzalutamide. As shown, treatment of SPOP-depleted C4-2 cells with enzalutamide reduced the level of both γH2AX and fluorescence intensity of TOP2A in the nuclei (Figure 6, A–D). The TOP2A knockdown in

SPOP-depleted C4-2 cells partially restored the level of γH2AX (Figure 6, E and F). These data suggest that the AR and TOP2A are critical for the generation of DNA breaks in SPOP-knockdown C4-2 cells. We also examined the level of γH2AX in AR–stably expressing PC3 and DU145 cells, both of which are originally AR negative. As shown, the level of γH2AX was not increased by SPOP knockdown in AR-expressing PC3 cells and DU145 cells (Supplemental Figure S6, A–D). These data suggest that the expression of AR alone was not sufficient for SPOP-mediated DSB repair, and other factors (e.g., cofactors for the AR/TOP2 interaction) may be necessary for the AR/TOP2A-mediated DSBs.

SPOP attenuates cytotoxicity of etoposide

Depletion of TDP1 or TDP2 causes hypersensitivity to etoposide (Nitiss *et al.*, 2006; Zeng *et al.*, 2011). Because SPOP positively regulates protein expression of TDP1/2 and is required for TOP2A removal from the TOP2A–DNA cleavage complex, we next examined the sensitivity to etoposide in SPOP-deficient or SPOP-proficient cells. The level of γH2AX was increased in a time-dependent manner by treatment of C4-2 cells with etoposide (Figure 7, A and B). In SPOP-depleted cells, the level of γH2AX was increased compared with that of control C4-2 cells before etoposide treatment (Figure 7, A and B). The level of γH2AX at 4 h after addition of etoposide was significantly higher in SPOP knockdown
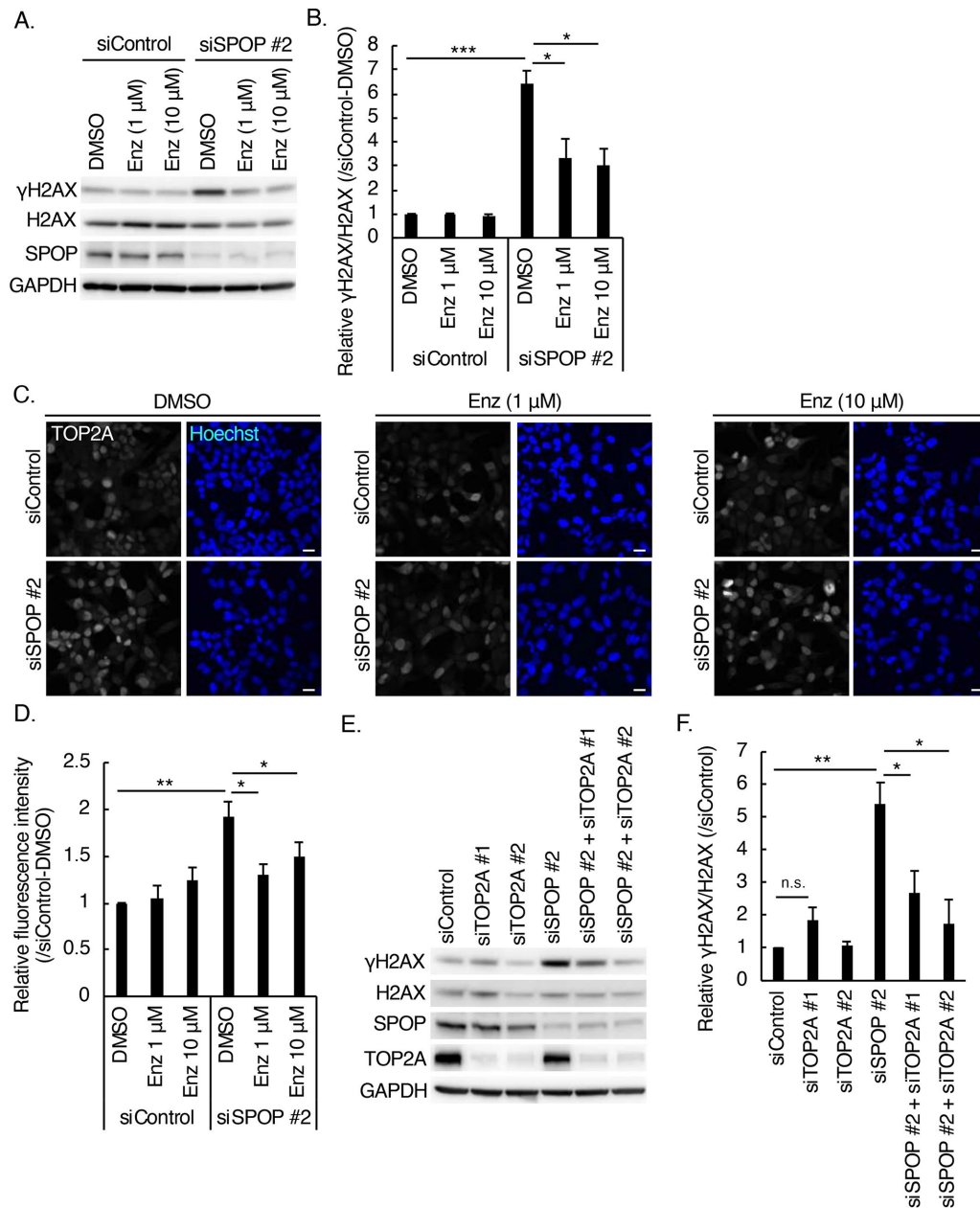
FIGURE 6: AR and TOP2A dependency on the increased level of γH2AX in SPOP-knockdown C4-2 cells. (A) Western blots of cell lysates prepared from control or SPOP-knockdown C4-2 cells incubated with an AR inhibitor, enzalutamide (Enz). Cells were treated with enzalutamide at the indicated concentrations in 10% FBS–containing medium for 48 h before cell lysis. (B) Quantitation of A. Ratio of γH2AX/H2AX was analyzed from three independent experiments. Data show the mean ± SEM. *, $p < 0.05$; ***, $p < 0.001$. (C) Confocal images of C4-2 cells fixed after 72 h transfection of siRNA, permeabilized, and stained for TOP2A antibody. Cells were treated with enzalutamide at the indicated concentrations in 10% FBS–containing medium for 48 h before fixation. Bars = 20 μm. (D) Quantitation of C. Fluorescence intensity of TOP2A in the nuclei was measured and normalized to that of control cells. In total, 50 cells were analyzed. Data show the mean ± SEM. *, $p < 0.05$; **, $p < 0.01$. (E) Western blots of C4-2 cell lysates 72 h posttransfection of siRNAs. (F) Quantitation of E. Ratio of γH2AX/H2AX was analyzed from three independent experiments. Data show the mean ± SEM. *, $p < 0.05$; **, $p < 0.01$; n.s., not significant.

cells than in control cells (Figure 7, A and B). Consistently, SPOP depletion significantly inhibited the cell proliferation of C4-2 cells, and treatment of SPOP-depleted C4-2 cells with etoposide drastically enhanced the cytotoxic effect of etoposide (Figure 7C). In C4-2 cells that overexpress WT SPOP, vice versa, the elevation of γH2AX was significantly suppressed at 24 h after addition of etoposide (Figure 7, D and E). Overexpression of WT SPOP partially attenu-

ated the inhibition of cell proliferation by etoposide treatment (Figure 7F). These data suggest that SPOP relieves the cytotoxicity of etoposide.

DISCUSSION

Genome instability (e.g., gene rearrangement and gene amplification) is a hallmark of various cancers (Hanahan and Weinberg, 2011).

FIGURE 7: Sensitivity to etoposide in SPOP-depleted and SPOP-overexpressing C4-2 cells. (A) Western blots of cell lysates prepared from control or SPOP-knockdown C4-2 cells incubated with 50 µM etoposide (Etop) for the indicated time in 10% FBS–containing medium. (B) Quantitation of A. Ratio of γH2AX/H2AX was analyzed from three independent experiments. Data show the mean ± SEM. *, $p < 0.05$; ***, $p < 0.001$. (C) Cell proliferation assay. Af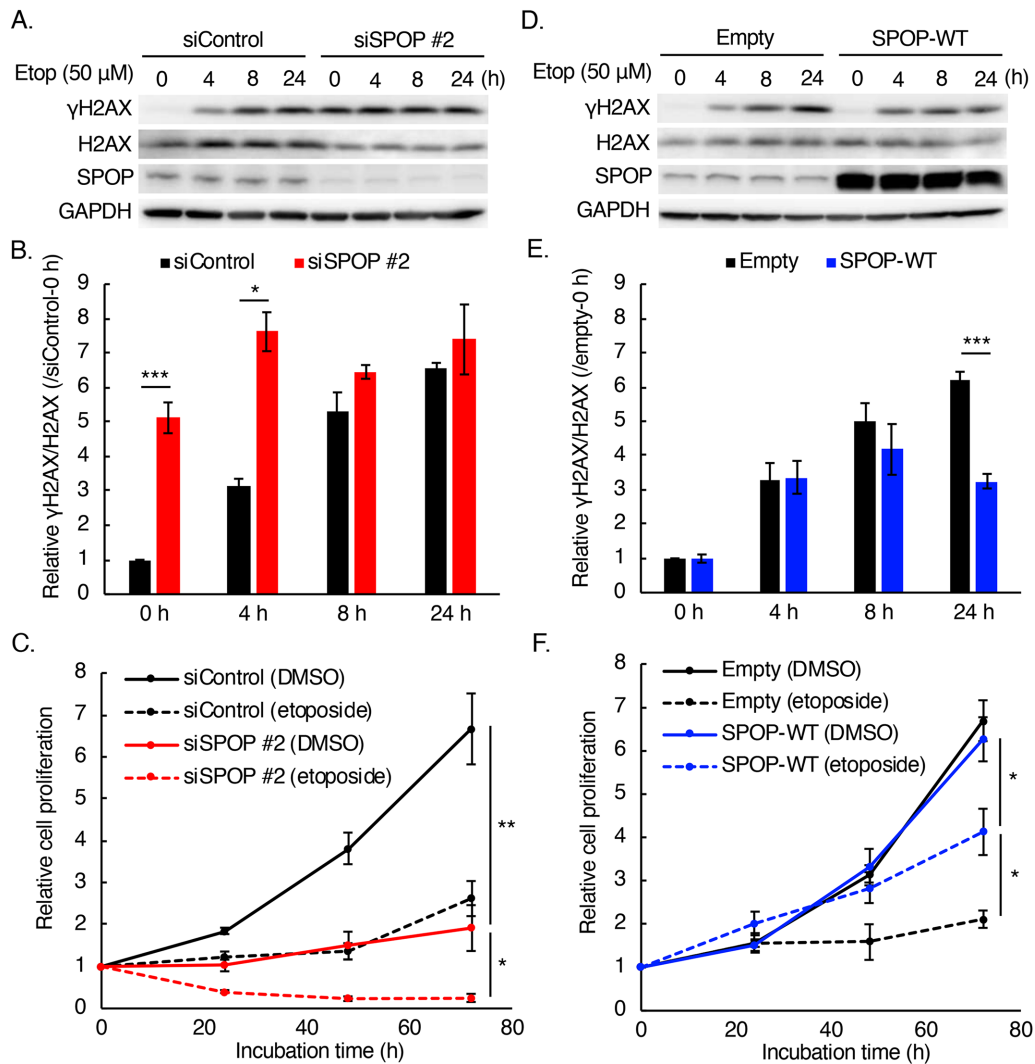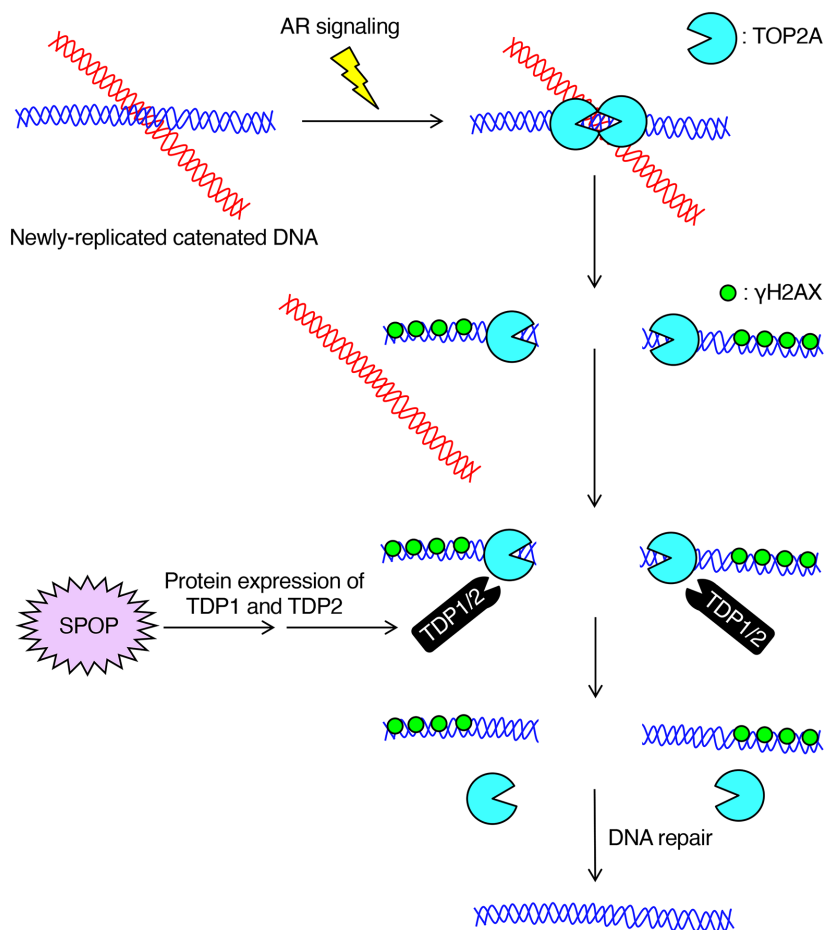ter 48 h transfection of siRNA in C4-2 cells, 50 µM etoposide was added in 10% FBS–containing medium. The cells were then counted every 24 h. Data are the mean ± SEM from three independent experiments. *, $p < 0.05$; **, $p < 0.01$. (D) Western blots of cell lysates prepared from control or nontagged SPOP WT-overexpressed C4-2 cells incubated with 50 µM etoposide (Etop) for the indicated time in 10% FBS–containing medium. Empty, control lentivirus. (E) Quantitation of D. The ratio of γH2AX/H2AX was analyzed from three independent experiments. Data show the mean ± SEM. ***, $p < 0.001$. Empty, control lentivirus. (F) Cell proliferation assay. After 48 h infection of lentivirus carrying nontagged SPOP WT in C4-2 cells, 50 µM etoposide was added in 10% FBS–containing medium. The cells were then counted every 24 h. Data are the mean ± SEM from three independent experiments. *, $p < 0.05$; Empty, control lentivirus.

In prostate cancer, the TMPRSS2 and ERG fusion gene was observed in nearly 50% of human prostate cancer patients (Tomlins *et al.*, 2005). Dysregulation of DNA repair often causes gene rearrangements (Burrell *et al.*, 2013). Previous studies have clearly shown that SPOP is essential for proper DNA repair process in response to exogenous DNA damage stresses such as γ or UV irradiation, and the addition of hydroxyurea or camptothecin (Boysen *et al.*, 2015; Hjorth-Jensen *et al.*, 2018). SPOP knockdown or overexpression of the prostate cancer–associated SPOP mutant, F133V, impaired HDR and enhanced NHEJ, which could generate gene rearrangement with higher frequency (Boysen *et al.*, 2015). SPOP is also essential for mRNA expression of ataxia telangiectasia and Rad3-related protein, BRCA2, checkpoint kinase 1, and Rad51,

which are essential for the proper progress of DNA repair (Hjorth-Jensen *et al.*, 2018). In the present study, in addition to these critical functions of SPOP during DNA repair, we showed that SPOP is also essential for DNA–protein cross-link repair in AR-positive prostate cancer cells. Accumulation of γH2AX was observed in SPOP-depleted C4-2 cells in the absence of exogenous DNA damage stresses. Our present study suggests that SPOP is necessary for dissociating TOP2A from genomic DNA through regulation of TDP1/2 protein expression (Figure 8). In SPOP-knockdown C4-2 cells, the protein expression of TDP1/2 was reduced without affecting their mRNA expression level (Figure 3, I–K). SPOP may ubiquitinate unidentified ubiquitin E3s for TDP1/2, leading to their proteasomal degradation. Recently, a deubiquitinase for TDP1,

FIGURE 8: Scheme of this study. During DNA replication, AR signaling enhances double-strand breaks by TOP2A to solve the topological issues of newly replicated DNA. In this process, SPOP is required for eliminating TOP2A from the TOP2A–DNA cleavage complex by regulating the protein expression of tyrosyl–DNA phosphodiesterases (TDP1 and TDP2).

SPOP, prostate cancer–associated SPOP mutants Y87C nor F133V affected the half-life of TOP2A protein (Supplemental Figure S7, B and C). Overexpression of WT SPOP did not increase the ubiquitination of TOP2A (Supplemental Figure S7D). The mRNA level of TOP2A was affected by overexpression of neither WT SPOP, Y87C, nor F133V mutant (Supplemental Figure S7E). These data suggest that increased TOP2A protein by overexpression of the F133V mutant is because of neither the inhibition of TOP2A protein degradation nor the increase of TOP2A mRNA expression. Overexpression of the F133V mutant may enhance the translation efficiency of TOP2A mRNA.

To date, all known prostate cancer–associated SPOP mutants including Y87C and F133V similarly fail to interact with its substrates, and expression of all SPOP mutants also equally causes the accumulation of the substrates because of the inhibition of their degradation. Here, we found that overexpression of the F133V mutant increased the level of γH2AX and fluorescence intensity of TOP2A in the nuclei much more than that of Y87C mutant did (Figures 4 and 5, C and D). Although the protein expression of TOP2A was slightly decreased by SPOP knockdown and not affected by Y87C mutant overexpression (Figures 3, C and D, and 4A and Supplemental Figure S5A), overexpression of the F133V mutant increased the protein expression of TOP2A (Figure 4A and Supplemental Figure S5A). The protein expression of MRE11 was decreased by overexpression of the F133V mutant, but not by SPOP knockdown or Y87C mutant overexpression (Figures 3, I and J, and 4A and Supplemental Figure S5A). These data suggest the distinct functions among prostate cancer–associated SPOP variants in the regulation of DNA–protein cross-link repair. It is likely that the F133V mutant may exert a dominant-negative effect on the down-regulation of TDP2 and a gain-of-function effect on the down-regulation of MRE11. SPOP is a substrate recognition receptor of the CUL3/RING ubiquitin E3 complex, and to date, approximately 30 proteins have been reported as its substrates (Cheng et al., 2018). F133V mutation is located in the substrate-binding domain of SPOP, and is supposed to interact with CUL3 as does WT SPOP. If the F133V mutant loses the binding affinity to substrates, the mutant is expected to serve as a dominant-negative mutant as reported previously (Cheng et al., 2018). If the F133V mutant acquires the ability to interact with proteins to which WT SPOP cannot bind, the mutant could exert gain-of-function effects. Our results may suggest unidentified substrates that the F133V mutant, but not WT SPOP, can recognize. Further studies are needed to characterize functions of the F133V mutant during the DNA–protein cross-link repair process.

UCHL3, has been identified (Liao et al., 2018). UCHL3 decreases the ubiquitination level of TDP1 leading to the inhibition of TDP1 degradation. Further studies would identify the ubiquitin E3s for TDP1/2 in the future.

In prostate cancer patients, protein expression of TOP2A correlated with increasing Gleason scores and a higher level of prostate-specific antigen (Willman and Holden, 2000; Hughes et al., 2006; de Resende et al., 2013). Both mRNA and protein expression of TOP2A is up-regulated in an aggressive prostate cancer subgroup (Labbe et al., 2017). Collaboration of TOP2A and AR signaling promotes prostate cancer progression by inducing gene rearrangements as well as TOP2B (Haffner et al., 2010; Schaefer-Klein et al., 2015). Taken together with our present results, accumulation of TOP2A on genomic DNA in prostate cancer patients carrying a F133V mutation in SPOP could frequently produce gene rearrangement, and contribute to prostate cancer progression. SPOP may thus prevent the development of prostate cancers by attenuating DNA replication stresses through the proper progress of TOP2A/TDP-dependent DNA–protein cross-link repair. Although human TOP2A possesses four SPOP recognizable degrons ([598]WKSST[602], [617]GTSTS[621], [687]GQTTT[691], and [916]LNSTT[920]) in its amino acid sequence, the interaction of TOP2A and SPOP was not detectable in C4-2 cells (Supplemental Figure S7A), suggesting that TOP2A would not be a direct target of SPOP. Overexpression of neither WT

MATERIALS AND METHODS
Antibodies
The following antibodies were purchased from the manufacturers as indicated: rabbit anti-SPOP antibody (16750-1-AP, dilution 1:1000 for Western blotting, immunofluorescence; Proteintech), rabbit anti-H2AX antibody (D17A3, dilution 1:1000; Cell Signaling Technology), mouse anti-γH2AX antibody (2F3, dilution 1:1000 for Western blotting, immunofluorescence; Biolegend), rabbit anti-ChK2 antibody (D9C6, dilution 1:1000; Cell Signaling Technology), rabbit anti-phosphorylated ChK2 antibody (C13C1, dilution 1:1000; Cell

Signaling Technology), rabbit anti-ATM antibody (D2E2, dilution 1:1000; Cell Signaling Technology), mouse anti-phosphorylated ATM antibody (10H11.E12, dilution 1:1000; Cell Signaling Technology), rabbit anti-EGFR (epidermal growth factor receptor) antibody (D38B1, dilution 1:1000; Cell Signaling Technology), rabbit anti-phosphorylated EGFR (Y1068) antibody (D7A5, dilution 1:1000; Cell Signaling Technology), rabbit anti-TOP1 antibody (ab109374, dilution 1:1000 for Western blotting, dilution 1:200 for immunofluorescence; Abcam), rabbit anti-TOP2A antibody (24641-1-AP, dilution 1:1000 for Western blotting, dilution 1:200 for immunofluorescence, dilution 1:500 for immunoprecipitation; Proteintech), rabbit anti-TOP2B antibody (MA5-24310, dilution 1:1000; Invitrogen), rabbit anti-MRE11 antibody (31H4, dilution 1:1000; Cell Signaling Technology), rabbit anti-TDP1 antibody (D8D1B, dilution 1:1000; Cell Signaling Technology), mouse anti-TDP2 antibody (TA811981, dilution 1:1000; Thermo), rabbit anti-AR antibody (ab133273, dilution 1:1000; Abcam), mouse anti-His antibody (9C11, dilution 1:3000; Wako), mouse anti-FLAG antibody (M2, dilution 1:1000; Sigma), mouse anti-GAPDH antibody (5A12, dilution 1:6000; Wako), rabbit normal immunoglobulin G (IgG) (2729; Cell Signaling Technology), goat Cy3-conjugated anti-rabbit IgG antibody (A10520, dilution 1:2000; Molecular Probes), goat Alexa 488–conjugated anti-mouse IgG antibody (A11001, dilution 1:2000; Molecular Probes), horseradish peroxidase (HRP)-conjugated anti-mouse IgG antibody (W4021, dilution 1:2000; Promega) and HRP-conjugated anti-rabbit IgG antibody (W4011, dilution 1:2000; Promega).

Plasmids

SPOP was amplified with the Halo-SPOP vector (FHC02905; Promega) using the following pairs of primers: 5'-ATGTCAAGGGTTCCAAGTCC-3' (SPOP sense primer), 5'-TTAGGATTGCTTCAGGCGTT-3' (SPOP antisense primer). His-Ub (ubiquitin) was amplified with the HA-Ub vector (a kind gift from Tatsuya Sawasaki, Ehime University) using the following pairs of primers: 5'-ATGCATCACCATCACCATCACATGCAGATCTTCGTGAAGAC-3' (His-Ub sense primer), 5'-TTACCCACCTCTGAGACGGA-3' (Ub antisense primer). AR-FLAG was amplified with the AR-FLAG vector (a kind gift from Yuuki Imai, Ehime University) using the following pairs of primers: 5'-ATGGAAGTGCAGTTAGGGCT-3' (AR sense primer), 5'-TTACTTGTCATCGTCGTCCTTGTAGTC-3' (FLAG antisense primer). The PCR products were introduced into the blunt end of the CSII-CMV-MCS-IRES2-Bsd vector. The SPOP mutant vectors were produced using the following pairs of primers: 5'-CTGTCACTTTGCCTGTTACTGGTCA-3' (SPOP-Y87C sense primer), 5'-GTAATCTTTGCTTTCTTCATCTAAC-3' (SPOP-Y87C antisense primer), 5'-GCAAAGACTGGGGAGTCAAGAAATT-3' (SPOP-F133V sense primer), 5'-CTTGCACAAACCTATATGCCCGTTG-3' (SPOP-F133V antisense primer). The siRNA-resistant SPOP vectors were produced by overlapping PCR using the following pairs of primers: 5'-GCGAAAGGTGAGGAGACGAAGGCAATGGAGAGTCAACGGGCATAT-3' (SPOP-F2 sense primer) and 5'-TTAGGATTGCTTCAGGCGTT-3' (SPOP antisense primer); 5'-ATGTCAAGGGTTCCAAGTCC-3' (SPOP sense primer) and 5'-TTGCCTTCGTCTCCTCACCTTTCGCATTCAGGATGGAGAATTTGA-3' (SPOP-R2 antisense primer).

Cell culture

C4-2 cells, LNCaP cells, PC3 cells, and DU145 cells were purchased from the American Type Culture Collection and maintained at 37°C with 5% CO$_2$ in RPMI (Wako) supplemented with 10% fetal bovine serum (FBS), 20 U/ml penicillin, and 100 µg/ml streptomycin. HEK293T cells were maintained at 37°C with 5% CO$_2$ in DMEM (Wako) supplemented with 10% FBS, 20 U/ml penicillin, and 100 µg/ml streptomycin. PC3 cells and DU145 cells that stably express AR-FLAG were established by the selection with 50 µg/ml blasticidin S (Wako) after infection of lentivirus carrying AR-FLAG gene. Cells were treated with 1–10 µM irinotecan (Wako) at 37°C for 24 h, 10–50 µM etoposide (Sigma) at 37°C for 24 h, 100–1000 µM hydroxyurea (Abcam) at 37°C for 24 h, 10 µM Ku55933 (Sigma) at 37°C for 24 h, 1–10 µM enzalutamide (ChemScene) at 37°C for 48 h, and 100 µM mirin (Sigma) at 37°C for 4 h. Cells were stimulated with 100 ng/ml EGF (R&D systems) in 2% FBS for 24–48 h. For the cycloheximide chase assay, cells were treated with 25 µg/ml cycloheximide (Sigma) at 37°C.

Transfection

For transfection of plasmids into HEK293T cells, GeneJuice (Millipore) was used according to the manufacturer's instructions. At 48 h posttransfection, cells were subjected to subsequent experiments. Transfections of siRNAs (10 nM) into prostate cancer cells were performed using RNAimax (Invitrogen) according to the manufacturer's instructions. Subsequent experiments were performed at 72 h posttransfection.

Lentiviral expression

Transient expression of SPOP was induced through the lentiviral infection as described previously (Tanigawa et al., 2019). Briefly, lentiviruses carrying SPOP (WT, Y87C, or F133V) were produced by transfection of those cDNA cloned into the CSII-CMV-MCS-IRES2-Bsd vector with two packaging vectors (the pCAG-HIVgp vector and pCMV-VSVG-RSV-Rev vector) in HEK293T cells. At 48 h posttransfection, lentiviruses in the medium were collected. The collected lentiviruses were added to the culture medium of the prostate cancer cells. Expression of SPOP (WT, Y87C, or F133V) in prostate cancer cells was detected at 96 h after lentiviral infection. For rescue experiments, expression of SPOP was detected at 48 h after lentiviral infection. The CSII-CMV-MCS-IRES2-Bsd, pCAG-HIVgp, and pCMV-VSVG-RSV-Rev vectors were kind gifts from Hiroyuki Miyoshi (RIKEN).

siRNAs

The following validated siRNA duplex oligomers were purchased and used for knockdown experiments: ACACACAGAUCAAGGUAGUGAAAUU (siSPOP #1; Invitrogen), GCCAAGGGAGAAGAAACCAAAGCUA (siSPOP #2; Invitrogen), GCUCAGCUCUUUGGCUCGAUUGUUA (siTOP2A #1; Invitrogen), and CAACCUUCAACUAUCUUCUUGAUAU (siTOP2A #2; Invitrogen). Control siRNA were purchased from Sigma (SIC-001).

Western blotting and immunoprecipitation

Western blotting and immunoprecipitation were performed as described previously (Maekawa et al., 2017).

In vivo ubiquitination assay

The ubiquitination assay was performed as described previously (Maekawa et al., 2019).

Cell proliferation assay

The cell proliferation assay was performed as described previously with slight modifications (Murakami et al., 2019). Briefly, a total of 5×10^4 C4-2 cells were seeded into a 24-well plate in triplicate. Cells were treated with siRNA or infected with lentivirus the next day. After 48 h, cells were then treated with 50 µM etoposide in growth medium. At this time, the cells were counted (day 0). The cells were counted every 24 h after addition of etoposide.

RT-PCR

Total RNAs were extracted from prostate cancer cells using ISOGEN II (Nippon Gene) according to the manufacturer's protocol. The total RNA (1 μg) was used for cDNA synthesis using High Capacity RNA-to-cDNA Master Mix (Applied Biosystems). Real-time PCR (RT-PCR) was carried out (FastStart Universal SYBR Green Master ROX; Roche) on the ABI 7300/7500 Real-Time PCR system (Applied Biosystems) using the following pairs of primers: 5'-TACCTCACCGCT-GAGATCCT-3' (H2AX sense primer), 5'-AGCTTGTTGAGCTCCTC-GTC-3' (H2AX antisense primer), 5'-CGGCCTGTCCAGTTTGAAAT-3' (MRE11 sense primer), 5'-GTGGGATCGTCATGATTGCC-3' (MRE11 antisense primer), 5'-GCTTTGACGTGGACTGGCTCG-3' (TDP1 sense primer), 5'-GGCTTGGCCTGGGCATGGAGG-3' (TDP1 anti-sense primer), 5'-GCAAGAGGCTCCAGAGTCAGC-3' (TDP2 sense primer), 5'-GGCAATGTTTAGGTTTGCCC-3' (TDP2 antisense primer), 5'-GGTCCTGAAGATGATGCTGC-3' (TOP2A sense primer), 5'-GGAAGCCCAAGTAACTTTCG-3' (TOP2A antisense primer), 5'-TGCACCACCAACTGCTTAGC-3' (GAPDH sense primer), 5'-GGCATGGACTGTGGTCATGAG-3' (GAPDH antisense primer).

Immunofluorescence staining

Cells were fixed with 4% paraformaldehyde in phosphate-buffered saline (PBS) for 30 min at room temperature and permeabilized with 0.1% Triton X-100 in PBS for 15 min at room temperature. After blocking with 3% bovine serum albumin in PBS for 30 min at room temperature, cells were incubated with primary antibodies and then with secondary antibodies conjugated to fluorophores. To stain nuclei, fixed cells were treated with Hoechst33342 (dilution 1:2000; Molecular Probe) at room temperature for 1 h.

Confocal microscopy

Confocal microscopy was performed using the A1R laser confocal microscope (Nikon) with a 60× 1.27 Plan-Apochromat water immersion lens. Images were analyzed with ImageJ or Fiji software (National Institutes of Health).

Topoisomerase activities measurement

Cells were collected from three 10-cm dishes and centrifuged at $800 \times g$ for 3 min at 4°C. The pellet was resuspended in ice-cold TEMP buffer (10 mM Tris-HCl, pH 7.5, 1 mM EDTA, 4 mM $MgCl_2$, 0.5 mM phenylmethylsulfonyl fluoride [PMSF], protease inhibitor cocktail), and centrifuged at $800 \times g$ for 3 min at 4°C. The cell pellet was homogenized using a Dounce tight-fitting homogenizer, and centrifuged at $1500 \times g$ for 10 min at 4°C. The nuclear pellet was resuspended with equal volume of TEP buffer (10 mM Tris-HCl, pH 7.5, 1 mM EDTA, 0.5 mM PMSF) and 1 M NaCl. The suspension was subjected to ultracentrifugation at $100,000 \times g$ for 60 min at 4°C. The supernatant was used for topoisomerase activities measurement. The topoisomerase activities were then measured using the Topoisomerase I or II Assay Kit (TG1015-1 or TG1001-1, respectively; TopoGEN) according to the manufacturer's protocol.

Detection of the topoisomerase–DNA complex

Purification of genomic DNA was performed by cesium chloride–density gradient ultracentrifugation as described previously (Hoa et al., 2016). Cells were treated with 10 μM etoposide (Sigma) at 37°C for 2 h, or 100 μM mirin (Sigma) at 37°C for 4 h before cell lysis. After cesium chloride–gradient ultracentrifugation (total volume, 10 ml), a total of 1 ml was collected from the top to bottom (fraction #'s 1–10). One hundred microliters of each fraction was subjected to Western dot blotting, and the blot intensity of each fraction (#'s 1–10) was shown as the percentage of total blot intensity.

Statistical analysis

Statistical comparisons were made using the two-tailed Student's t test or one-way analysis of variance followed by Dunnett's post hoc test.

REFERENCES

An J, Wang C, Deng Y, Yu L, Huang H (2014). Destruction of full-length androgen receptor by wild-type SPOP, but not prostate-cancer-associated mutants. Cell Rep 6, 657–669.

Barbieri CE, Baca SC, Lawrence MS, Demichelis F, Blattner M, Theurillat JP, White TA, Stojanov P, Van Allen E, Stransky N, et al. (2012). Exome sequencing identifies recurrent SPOP, FOXA1 and MED12 mutations in prostate cancer. Nat Genet 44, 685–689.

Bartek J, Lukas C, Lukas J (2004). Checking on DNA damage in S phase. Nat Rev Mol Cell Biol 5, 792–804.

Boysen G, Barbieri CE, Prandi D, Blattner M, Chae SS, Dahija A, Nataraj S, Huang D, Marotz C, Xu L, et al. (2015). SPOP mutation leads to genomic instability in prostate cancer. eLife 4, e09207.

Burrell RA, McGranahan N, Bartek J, Swanton C (2013). The causes and consequences of genetic heterogeneity in cancer evolution. Nature 501, 338–345.

Cheng J, Guo J, Wang Z, North BJ, Tao K, Dai X, Wei W (2018). Functional analysis of Cullin 3 E3 ligases in tumorigenesis. Biochim Biophys Acta 1869, 11–28.

Delgado JL, Hsieh CM, Chan NL, Hiasa H (2018). Topoisomerases as anticancer targets. Biochem J 475, 373–398.

de Resende MF, Vieira S, Chinen LT, Chiappelli F, da Fonseca FP, Guimaraes GC, Soares FA, Neves I, Pagotty S, Pellionisz PA, et al. (2013). Prognostication of prostate cancer based on TOP2A protein and gene assessment: TOP2A in prostate cancer. J Transl Med 11, 36.

Dupre A, Boyer-Chatenet L, Sattler RM, Modi AP, Lee JH, Nicolette ML, Kopelovich L, Jasin M, Baer R, Paull TT, Gautier J (2008). A forward chemical genetic screen reveals an inhibitor of the Mre11-Rad50-Nbs1 complex. Nat Chem Biol 4, 119–125.

Gaillard H, Garcia-Muse T, Aguilera A (2015). Replication stress and cancer. Nat Rev Cancer 15, 276–289.

Gan W, Dai X, Lunardi A, Li Z, Inuzuka H, Liu P, Varmeh S, Zhang J, Cheng L, Sun Y, et al. (2015). SPOP promotes ubiquitination and degradation of the ERG oncoprotein to suppress prostate cancer progression. Mol Cell 59, 917–930.

Haffner MC, Aryee MJ, Toubaji A, Esopi DM, Albadine R, Gurel B, Isaacs WB, Bova GS, Liu W, Xu J, et al. (2010). Androgen-induced TOP2B-mediated double-strand breaks and prostate cancer gene rearrangements. Nat Genet 42, 668–675.

Hanahan D, Weinberg RA (2011). Hallmarks of cancer: the next generation. Cell 144, 646–674.

Hjorth-Jensen K, Maya-Mendoza A, Dalgaard N, Sigurethsson JO, Bartek J, Iglesias-Gato D, Olsen JV, Flores-Morales A (2018). SPOP promotes transcriptional expression of DNA repair and replication factors to prevent replication stress and genomic instability. Nucleic Acids Res 46, 9484–9495.

Hoa NN, Shimizu T, Zhou ZW, Wang ZQ, Deshpande RA, Paull TT, Akter S, Tsuda M, Furuta R, Tsutsui K, et al. (2016). Mre11 is essential for the removal of lethal topoisomerase 2 covalent cleavage complexes. Mol Cell 64, 580–592.

Hughes C, Murphy A, Martin C, Fox E, Ring M, Sheils O, Loftus B, O'Leary J (2006). Topoisomerase II-α expression increases with increasing Gleason

score and with hormone insensitivity in prostate carcinoma. J Clin Pathol 59, 721–724.

Koc A, Wheeler LJ, Mathews CK, Merrill GF (2004). Hydroxyurea arrests DNA replication by a mechanism that preserves basal dNTP pools. J Biol Chem 279, 223–230.

Kwon JE, La M, Oh KH, Oh YM, Kim GR, Seol JH, Baek SH, Chiba T, Tanaka K, Bang OS, et al. (2006). BTB domain-containing speckle-type POZ protein (SPOP) serves as an adaptor of Daxx for ubiquitination by Cul3-based ubiquitin ligase. J Biol Chem 281, 12664–12672.

Labbe DP, Sweeney CJ, Brown M, Galbo P, Rosario S, Wadosky KM, Ku SY, Sjostrom M, Alshalalfa M, Erho N, et al. (2017). TOP2A and EZH2 provide early detection of an aggressive prostate cancer subgroup. Clin Cancer Res 23, 7072–7083.

Lee CL, Lin YT, Chang FR, Chen GY, Backlund A, Yang JC, Chen SL, Wu YC (2012a). Synthesis and biological evaluation of phenanthrenes as cytotoxic agents with pharmacophore modeling and ChemGPS-NP prediction as topo II inhibitors. PLoS One 7, e37897.

Lee KC, Padget K, Curtis H, Cowell IG, Moiani D, Sondka Z, Morris NJ, Jackson GH, Cockell SJ, Tainer JA, Austin CA (2012b). MRE11 facilitates the removal of human topoisomerase II complexes from genomic DNA. Biol Open 1, 863–873.

Lee JH, Paull TT (2004). Direct activation of the ATM protein kinase by the Mre11/Rad50/Nbs1 complex. Science 304, 93–96.

Lee JH, Paull TT (2005). ATM activation by DNA double-strand breaks through the Mre11-Rad50-Nbs1 complex. Science 308, 551–554.

Liao C, Beveridge R, Hudson JJR, Parker JD, Chiang SC, Ray S, Ashour ME, Sudbery I, Dickman MJ, El-Khamisy SF (2018). UCHL3 regulates topoisomerase-induced chromosomal break repair by controlling TDP1 proteostasis. Cell Rep 23, 3352–3365.

Maekawa M, Hiyoshi H, Nakayama J, Kido K, Sawasaki T, Semba K, Kubota E, Joh T, Higashiyama S (2019). Cullin-3/KCTD10 complex is essential for K27-polyubiquitination of EIF3D in human hepatocellular carcinoma HepG2 cells. Biochem Biophys Res Commun 516, 1116–1122.

Maekawa M, Tanigawa K, Sakaue T, Hiyoshi H, Kubota E, Joh T, Watanabe Y, Taguchi T, Higashiyama S (2017). Cullin-3 and its adaptor protein ANKFY1 determine the surface level of integrin β1 in endothelial cells. Biol Open 6, 1707–1719.

Miskimins R, Miskimins WK, Bernstein H, Shimizu N (1983). Epidermal growth factor-induced topoisomerase(s). Intracellular translocation and relation to DNA synthesis. Exp Cell Res 146, 53–62.

Murai J, Huang SY, Das BB, Dexheimer TS, Takeda S, Pommier Y (2012). Tyrosyl-DNA phosphodiesterase 1 (TDP1) repairs DNA damage induced by topoisomerases I and II and base alkylation in vertebrate cells. J Biol Chem 287, 12848–12857.

Murakami A, Maekawa M, Kawai K, Nakayama J, Araki N, Semba K, Taguchi T, Kamei Y, Takada Y, Higashiyama S (2019). Cullin-3/KCTD10 E3 complex is essential for Rac1 activation through RhoB degradation in human epidermal growth factor receptor 2-positive breast cancer cells. Cancer Sci 110, 650–661.

Nitiss KC, Malik M, He X, White SW, Nitiss JL (2006). Tyrosyl-DNA phosphodiesterase (Tdp1) participates in the repair of Top2-mediated DNA damage. Proc Natl Acad Sci USA 103, 8953–8958.

Pommier Y, Huang SY, Gao R, Das BB, Murai J, Marchand C (2014). Tyrosyl-DNA-phosphodiesterases (TDP1 and TDP2). DNA Repair 19, 114–129.

Pommier Y, Sun Y, Huang SN, Nitiss JL (2016). Roles of eukaryotic topoisomerases in transcription, replication and genomic stability. Nat Rev Mol Cell Biol 17, 703–721.

Schaefer-Klein JL, Murphy SJ, Johnson SH, Vasmatzis G, Kovtun IV (2015). Topoisomerase 2 alpha cooperates with androgen receptor to contribute to prostate cancer progression. PLoS One 10, e0142327.

Smith J, Tho LM, Xu N, Gillespie DA (2010). The ATM-Chk2 and ATR-Chk1 pathways in DNA damage signaling and cancer. Adv Cancer Res 108, 73–112.

Stingele J, Bellelli R, Boulton SJ (2017). Mechanisms of DNA-protein crosslink repair. Nat Rev Mol Cell Biol 18, 563–573.

Tanigawa K, Maekawa M, Kiyoi T, Nakayama J, Kitazawa R, Kitazawa S, Semba K, Taguchi T, Akita S, Yoshida M, et al. (2019). SNX9 determines the surface levels of integrin β1 in vascular endothelial cells: implication in poor prognosis of human colorectal cancers overexpressing SNX9. J Cell Physiol 234, 17280–17294.

Theurillat JP, Udeshi ND, Errington WJ, Svinkina T, Baca SC, Pop M, Wild PJ, Blattner M, Groner AC, Rubin MA, et al. (2014). Prostate cancer. Ubiquitylome analysis identifies dysregulation of effector substrates in SPOP-mutant prostate cancer. Science 346, 85–89.

Tomlins SA, Rhodes DR, Perner S, Dhanasekaran SM, Mehra R, Sun XW, Varambally S, Cao X, Tchinda J, Kuefer R, et al. (2005). Recurrent fusion of TMPRSS2 and ETS transcription factor genes in prostate cancer. Science 310, 644–648.

Willman JH, Holden JA (2000). Immunohistochemical staining for DNA topoisomerase II-alpha in benign, premalignant, and malignant lesions of the prostate. Prostate 42, 280–286.

Zeng Z, Cortes-Ledesma F, El Khamisy SF, Caldecott KW (2011). TDP2/TTRAP is the major 5′-tyrosyl DNA phosphodiesterase activity in vertebrate cells and is critical for cellular resistance to topoisomerase II-induced DNA damage. J Biol Chem 286, 403–409.